Hindawi
Advances in Civil Engineering
Volume 2019, Article ID 6980782, 17 pages
https://doi.org/10.1155/2019/6980782

Research Article

Flexural Performance of Cross-Laminated Bamboo (CLB) Slabs and CFRP Grid Composite CLB Slabs

Qingfang Lv, Weiyang Wang, and Ye Liu

Key Laboratory of Concrete and Prestressed Concrete Structures of the Ministry of Education, Southeast University, Nanjing 210096, China

Correspondence should be addressed to Qingfang Lv; southeast_uni@126.com

Received 20 June 2019; Accepted 4 October 2019; Published 3 November 2019

Academic Editor: Claudio Mazzotti

In order to accord well with the requirements of sustainable development and green construction, a cross-laminated bamboo composed of an odd number of orthogonally oriented layers of bamboo scrimber is proposed in this paper. Adjacent bamboo layers are face-bonded by structural adhesives under pressure. The uniform mechanical and physical properties can be obtained through the orthogonal layup. Flexural performances of three groups of one-way CLB slabs and two groups of one-way CLB slabs strengthened with CFRP grids were investigated via four-point monotonic loading configuration until failure. Experimental parameters of thickness of the layer, number of layers, and manufacturing processes of CFRP grids were taken into consideration. Experimental observations showed that the failure of the CLB slab was brittle, and different failure modes were found in the CLB slab with CFRP grids via different manufacturing processes. Test results showed that the load-carrying capacity increased with the thickness of the layer, number of layers, and application of CFRP grids pressed in the bamboo layer, but the CFRP grids pressed in the interface of adjacent bamboo layers weakened the load-carrying capacity. The strain analysis demonstrated that the compression region was utilized with more efficiency via CFRP grids pressed in the bamboo layer, and the plane cross section assumption is suitable for both CLB slab and CLB slab strengthened with CFRP grids. A theoretical calculation method of flexural load-carrying capacity was proposed for the CLB slab, the accuracy of which was proved.

1. Introduction

In order to accord well with the requirements of sustainable development and green construction, the construction industry is undergoing significant modification and improvement [1]. More environment-friendly, durable, and less-labor materials are required to be adopted. A typical biological material, wood, has been widely used in civil construction, car industry, furniture industry [2–4], which satisfies above requirements. One of the most promising engineered wood products is cross-laminated timber (CLT). CLT consists of an odd number of orthogonally oriented layers of timber lumber [5], and adjacent layers are face-bonded via structural adhesives under pressure [6]. This specific configuration provides CLT with excellent in-plane and out-of-plane strength, rigidity, and stability [1], suitable for load-bearing panels and shear walls [7].

There are still many disadvantages of wood including a long growth, slow regeneration, a significant shortage, and a low utilization rate of the raw materials [8, 9]. Therefore, it is necessary to explore more feasible and appropriate materials based on sustainable requirements, and the bamboo is attracting researchers' attention. Compared with wood, advantages of the bamboo are demonstrated as follows: (1) faster growth speed, (2) high specific strength, (3) high specific rigidity, and (4) lower water swelling ratio [8–10]. The bamboo is convenient to be locally obtained in China, which has characteristics as saving costs, environmental friendliness, and recyclability [11–13]. However, the mechanical properties of the raw and unprocessed bamboo material are unstable, with large discreteness [14]. Many inevitable defects can also be found in the unprocessed bamboo material, which results in a poor durability [15–17]. To utilize the advantages of the raw bamboo and improve its material stability and performance,

kinds of bamboo engineering material, including laminated bamboo [18, 19] and reconstituted bamboo [20, 21], have been proposed and studied, which are beneficial to reduce the material discreteness and enlarge practical applications of the bamboo [22].

Inspired by the research studies on CLT, an upgraded cross-laminated bamboo is proposed in this paper, which has characteristics as uniform mechanical and physical properties due to orthogonal layup. Failure modes and flexural performance of three groups of the one-way CLB slab, a total of fifteen slab specimens, were discussed. Similar to generic CLT, the excessive deflection is prone to be found in the CLB under the out-of-plane loading [6], which makes the design controlled by the structural stiffness [23], limiting its structural application and wasting a large amount of strength capacity. Therefore, to further improve the practical utilization of the proposed CLB, strengthening techniques [24–27] are recommended, which are of important necessity. In wood structures, strengthening techniques include pre-stressed steel bar [24], carbon fiber-reinforced polymer (CFPR) sheet [28, 29], glass fiber-reinforced polymer (GFRP) sheet [30], and CFRP bar [31]. Wei et al. conducted a series of tests to study the effect of the steel bar and FRP sheet on the flexural performance of the bamboo scrimber beams [8]. Test results showed that the application of the fiber-reinforced polymer can be effective in improving the flexural performance of bamboo beams.

However, existing strengthening techniques with only one main force direction for wood structures are regarded as not suitable for CLBs with orthogonal force directions. A promising strengthening technique via FRP grids has been extensively investigated in concrete [32, 33], and it attracts the authors' attention in applying it to the CLB. The major concern is to achieve a good bond behavior between the FRP grids and CLB. In this paper, CFRP grids with high elastic modulus were considered, and two manufacturing process were adopted for applying CFRP grids to the CLB slab: (1) press the CFRP grids in the layer of the CLB slab and (2) press the CFRP grids in the interface of adjacent layers. The strengthening effectiveness of the CFRP grids on the CLB slab via different manufacturing processes was further evaluated.

2. Material

2.1. Bamboo Scrimber. Bamboo scrimber is a new type of engineering material, featured as having high material efficiency for utilizing almost 80% of raw bamboo inputs [34]. The process of the bamboo scrimber includes the following: (1) saturate the crushed moso bamboo strips with two-component polyurethane adhesive; (2) hot-press under a temperature of 140°C and a pressing rate of 1 minute to 2 minutes per millimeter; and (3) hot-cure and polish. The adopted process technology maintains the fibers' longitudinal direction and retains the basic characteristics of the bamboo. In this paper, the bamboo scrimber was manufactured by Hangzhou Dasuo Technology Co., Ltd., and had an average bulk density of 1200 kg/m^3.

Until now, no material test standard and codes have been published for bamboo scrimbers in China; therefore, the tensile, compressive, and flexural material tests on the bamboo scrimber were conducted based on the standards for measuring wood properties [35–37], and the dimensions of the tension specimens are shown in Figure 1. A total of ten tension specimens were prepared for measuring tensile properties parallel to grain and tensile properties perpendicular to grain, respectively. Each type of test contained five tension specimens. The tensile test was concentrically tested by the WDW-100E electronic universal testing machine depicted in Figure 2, and the test results related to tensile tests are listed in Table 1. The ultimate tensile stress parallel to grain (f_{ta}) and elastic modulus parallel to grain (E_{ta}) of the bamboo scrimber are 47.45 MPa and 17.95 GPa, respectively. The ultimate tensile stress perpendicular to grain (f_{tb}) and elastic modulus perpendicular to grain (E_{tb}) of the bamboo scrimber are 7.86 MPa and 3.75 GPa, respectively. The failure of the bamboo scrimber under tension includes tension rupture and shear-tension failure in the weakened region.

Referencing GB/T 1935-2009 "Method of testing in compressive strength parallel to grain of wood" [38] and GB/T 1939-2009 "Method of testing in compression perpendicular to grain of wood" [39], the dimensions of the compression specimens are shown in Figure 3. A total of ten compression specimens were prepared for measuring compressive properties parallel to grain and compressive properties perpendicular to grain, respectively. Each type of test contained five compression specimens. The compressive test was also tested by the WDW-100E electronic universal testing machine depicted in Figure 4, and the test results related to compressive tests are listed in Table 1. The ultimate compressive stress parallel to grain (f_{ca}), elastic modulus parallel to grain (E_{ca}), ultimate compressive stress perpendicular to grain (f_{cb}), and elastic modulus perpendicular to grain (E_{cb}) of the bamboo scrimber are 107.99 MPa, 21.55 GPa, 51.64 MPa, and 6.37 GPa, respectively. For the compression parallel to grain, the failure modes of the bamboo scrimber mainly are bond failure and local shear failure, as shown in Figure 5(a), and the former failure mode is mainly caused by processing quality problems such as uneven dipping and hot pressing. For the compression perpendicular to grain, the failure modes of the bamboo scrimber mainly are split and shear failure, depicted in Figure 5(b), regarded as brittle failure.

2.2. Fiber-Reinforced Polymer. Fiber-reinforced polymer has been extensively investigated, types of which include aramid, glass, carbon, basalt, and graphite [8]. Among various fiber-reinforced polymers, carbon fibre-reinforced polymer (CFRP) has been popular in recent years because of its excellent in-plane mechanical properties (such as stiffness and strength) and lightness [40]. Based on this, the CFRP is selected to form a grid network in this study, recognized as CFRP grids [41], which was fabricated by Nanjing Nortai Composite Material Equipment Manufacturing Co., Ltd. The adopted CFRP grids have three epoxy resin-glued layers

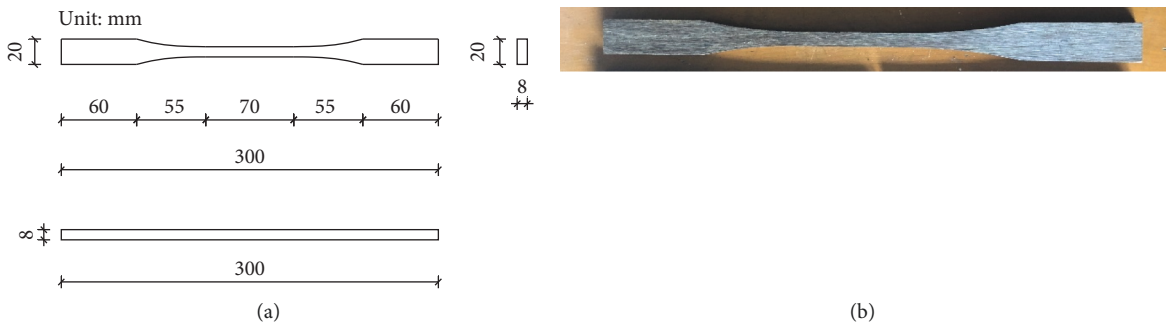

Figure 1: Tension specimen: (a) dimensions and (b) processed.

Figure 2: Tension test of the bamboo scrimber.

Table 1: Material properties of the bamboo scrimber.

Property	Average value	Standard deviation	Coefficient of variation (%)
Tensile test results			
Ultimate tensile stress parallel to grain (MPa)	47.45	8.81	18.57
Modulus of elasticity parallel to grain (GPa)	17.95	0.86	4.78
Ultimate tensile stress perpendicular to grain (MPa)	7.86	1.04	13.19
Modulus of elasticity perpendicular to grain (GPa)	3.75	0.33	8.89
Compressive test results			
Ultimate compressive stress parallel to grain (MPa)	107.99	7.78	7.20
Modulus of elasticity parallel to grain (GPa)	21.55	1.16	5.38
Ultimate compressive stress perpendicular to grain (MPa)	51.64	3.36	6.51
Modulus of elasticity perpendicular to grain (GPa)	6.37	0.61	9.65

in the longitudinal direction and two epoxy resin-glued layers in the transverse direction. The thickness and width of the single layer of CFRP reinforcement are about 0.7 mm and 7 mm, respectively. Based on ACI 440.3R-04 "Guide Test Methods for Fiber-Reinforced Polymers (FRPs) for Reinforcing or Strengthening Concrete Structures" [42], the uniaxial tensile tests were conducted on two layers and three layers of CFRP reinforcements via the WDW-100E electronic universal testing machine at a loading rate of 0.01 kN/s, respectively, and each series of CFRP tension specimens had five specimens. The dimension and test setup for CFRP tension specimens are shown in Figures 6 and 7, respectively.

The average ultimate tensile stress and modulus of elasticity for two-layer CFRP and three-layer CFRP are listed

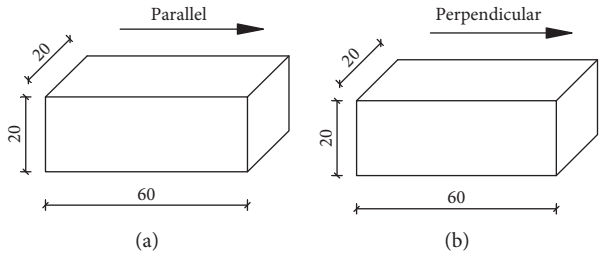

Figure 3: Compression specimen. (a) Parallel to grain. (b) Perpendicular to grain.

Figure 4: Compression test of the bamboo scrimber.

(a) (b)

Figure 5: Failure modes of the bamboo scrimber under compression. (a) Parallel to grain. (b) Perpendicular to grain.

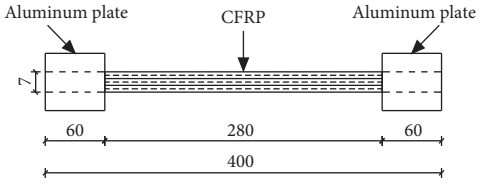

Figure 6: Dimensions of CFRP.

Table 2. For two-layer CFRP, the ultimate tensile stress and modulus of elasticity are 1141.52 MPa and 255.50 GPa, respectively. For three-layer CFRP, the ultimate tensile stress and modulus of elasticity are 952.57 MPa and 260.33 GPa, respectively. CFRP failed due to the fracture of CFRP fibers, as shown in Figure 8.

3. Experimental Program

3.1. Specimen Preparation. Three groups of one-way cross-laminated bamboo (CLB) slabs and two groups of one-way CLB slabs strengthened with CFRP grids are discussed in this paper. Each group consisted of five test specimens with identical parameters to take the material deviation and fabrication discreteness into consideration, which demonstrated that a total of twenty-five test specimens were studied. The key experimental parameters include the thickness of the layer, number of layers, CFRP grids, and corresponding manufacturing processes.

3.1.1. Details of One-Way CLB Slab. The dimensions and details of three groups of one-way CLB slabs, recognized as

Figure 7: Tension test of CFRP.

Figure 8: Failure picture of CFRP.

Table 2: Material properties of CFRP.

Property	Average value	Standard deviation	Coefficient of variation (%)
Two layers			
Ultimate tensile stress (MPa)	1141.52	53.32	4.67
Modulus of elasticity (GPa)	255.50	58.99	23.09
Three layers			
Ultimate tensile stress (MPa)	952.57	62.97	6.61
Modulus of elasticity (GPa)	260.33	55.62	21.37

CLB-A, CLB-B, and CLB-C, are shown in Figure 9 and listed in Table 3. In group CLB-A, the one-way CLB slab is composed of five 20 mm layers ($t_1 = t_2 = 20$ mm). In group CLB-B, the one-way CLB slab has seven layers. The thickness of outermost layers is $t_1 = 20$ mm while the thickness of middle layers is reduced to $t_2 = 12$ mm. For group CLB-C, the one-way CLB slab is composed of five 12 mm layers ($t_1 = t_2 = 12$ mm). The dimensions of groups CLB-A and CLB-B are designed as 1800 mm in length (l), 600 mm in width (b), and 100 mm in thickness (t), while the dimensions of group CLB-C are designed as 1800 mm in length (l), 600 mm in width (b), and 60 mm in thickness (t). In Table 3, the numbers 1–5 denote the five specimens with identical parameters in each group.

3.1.2. Details of One-Way CLB Slab Strengthened with CFRP Grids. In order to conveniently analyze the contribution of the CFRP grids for the flexural performance of the one-way CLB slab, the dimensions of the two groups of one-way CLB slabs strengthened with CFRP grids, designated as CLB-I and CLB-M, are kept the same with the groups CLB-A and CLB-C, respectively. The dimensions and details of one-way CLB slabs strengthened with CFRP grids are depicted in Figure 10 and presented in Table 4.

There are two strategies in composing the CFRP grids into the one-way CLB slab: (1) placing the CFRP grids into the bottom layer and hot-pressing both of the CFRP grids and bottom layer into an integrated whole, recognized as manufacturing process I, and (2) placing the CFRP grids between the bottom layer and penultimate layer and gluing and hot-pressing the CFRP grids and one-way CLB slab together, recognized as manufacturing process M. As mentioned in Section 2.2, the CFRP grids have three glued layers in the length direction and two glued layers in the width direction. The spacing of the CFRP grids is chosen as 50 mm × 50 mm.

3.1.3. Specimen Fabrication Process. As shown in Figures 9 and 10, the CLB slab is glued by multiple bamboo layers, and the angle between two adjacent layers is 90 degrees in terms of the bamboo fibers' arrangement direction. The bamboo fibers parallel to grain are designed as the length direction of outermost layers (top and bottom layers) in the one-way CLB slab. All CLB slabs were fabricated in Hangzhou Dasuo Technology Co., Ltd., China. The main processes of the one-way CLB slab and CLB slab strengthened with CFRP grids are shown in Figure 11.

3.2. Test Protocol. All twenty-five one-way CLB slab specimens strengthened with or without CFRP grids were tested under a four-point monotonic loading configuration until failure, as demonstrated in Figure 12. Before the formal loading, a 10 kN preload was applied to the specimen and was sustained about 3 minutes to verify the workability of the equipment. Then, the specimen was loaded at a loading rate of 5 kN per minute until failure. All slab specimens had a

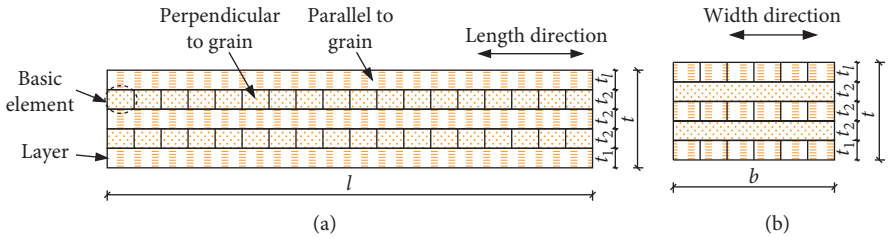

Figure 9: Details of one-way CLB slabs.

Table 3: Dimensions of one-way CLB slabs.

Group	Specimen	$l \times b \times t$ (mm)	t_1 (mm)	t_2 (mm)	N_l
CLB-A	CLB-A1, CLB-A2, CLB-A3, CLB-A4, CLB-A5	$1800 \times 600 \times 100$	20	20	5
CLB-B	CLB-B1, CLB-B2, CLB-B3, CLB-B4, CLB-B5	$1800 \times 600 \times 100$	20	12	7
CLB-C	CLB-C1, CLB-C2, CLB-C3, CLB-C4, CLB-C5	$1800 \times 600 \times 60$	12	12	5

Note. t_1 is the thickness of the outermost layer, as shown in Figure 9; t_2 is the thickness of the middle layer, as shown in Figure 9; N_l is the number of layers in one CLB slab.

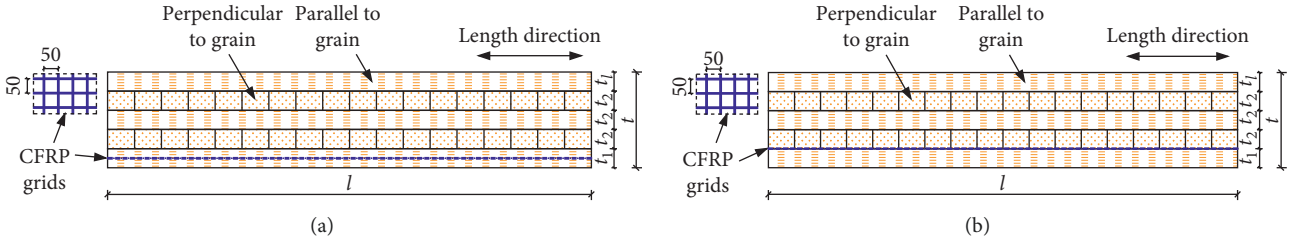

Figure 10: Details of one-way CLB slabs strengthened with CFRP grids: (a) CLB-I and (b) CLB-M.

Table 4: Dimensions of one-way CLB slabs strengthened with CFRP grids.

Group	Specimen	$l \times b \times t$ (mm)	t_1 (mm)	t_2 (mm)	N_l
CLB-I	CLB-I1, CLB-I2, CLB-I3, CLB-I4, CLB-I5	$1800 \times 600 \times 100$	20	20	5
CLB-M	CLB-M1, CLB-M2, CLB-M3, CLB-M4, CLB-M5	$1800 \times 600 \times 60$	12	12	5

clear span, L, of 1700 mm (distance between two supports) and a shear span, L_s, of 550 mm (distance from the support to the nearest loading point).

The layout of strain gages and displacement transducers is shown in Figure 13, which is same in all specimens. A total of five displacement transducers were adopted. Two displacement transducers were installed at the supports to monitor the vertical displacement of the slab specimen at the position of supports due to the flexural deformation. Two displacement transducers were employed at the loading points to monitor the displacements of loading points, and one displacement transducer was placed in the middle of the slab specimen to monitor the midspan displacement. The data of displacements obtained from the positions of supports and midspan were collected for calculating the clear deflection at the midspan of the slab specimen.

As shown in Figure 13, three strain gages were attached on the top and bottom slab surfaces at the midspan cross section to measure the tensile and compressive strains. Six equally spaced strain gages were attached on the side slab surface to monitor the strain variation along the slab thickness and change in height of the neutral axis. The load applied by the actuator was transferred from the force-transferring beam to the slab specimens, values of which were directly recorded by the testing machine. All data of displacements and strains were automatically collected by the KD7024 static strainmeter.

4. Test Results and Discussions

4.1. Experimental Observations and Failure Modes. The experimental observations and failure modes of one-way CLB slabs and CFRP grid-strengthened CLB slabs are depicted in Figures 14 and 15, respectively.

For the one-way CLB slab without CFRP grids, the typical failure process is demonstrated by taking group CLB-A with five 20 mm layers as an example. The deflection of the slab specimen slowly developed until the proportional limit. The small noise of the fracture of bamboo fibers was heard at the load of 100 kN, and small cracks were observed at the

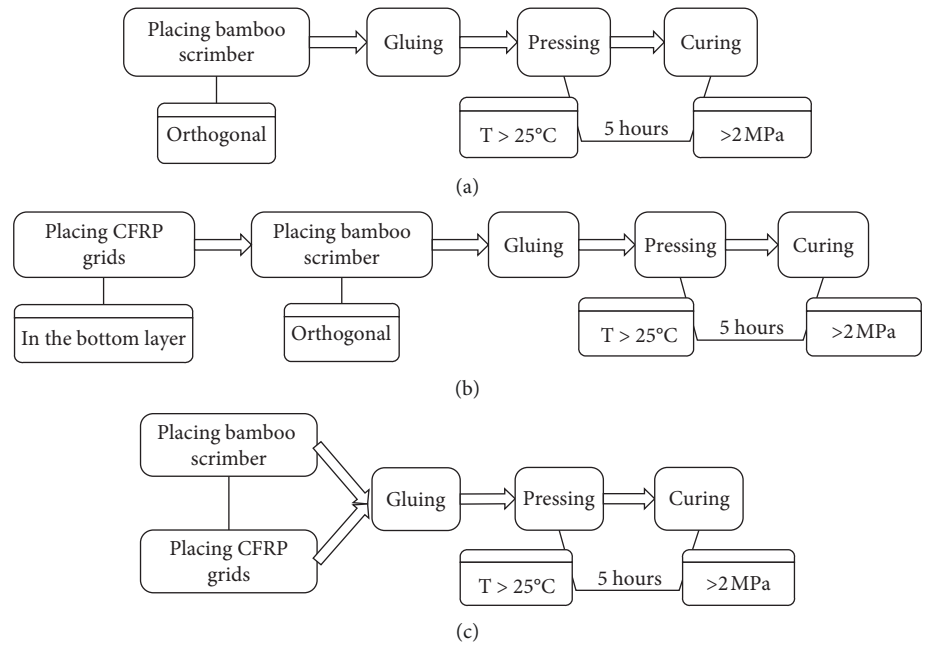

Figure 11: Fabrication processes of slab specimens. (a) One-way CLB slab. (b) One-way CLB slab strengthened with CFRP grids: manufacturing process I. (c) One-way CLB slab strengthened with CFRP grids: manufacturing process M.

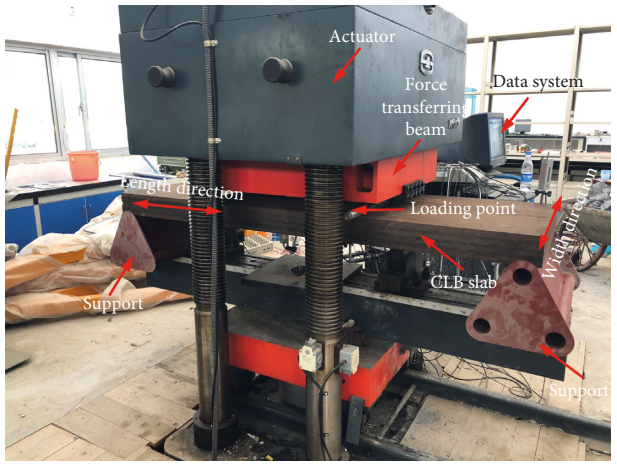

Figure 12: Test setup.

bottom surface of the slab specimen at the position of loading point or midspan. With the further increase of load, both displacement and cracks gradually grew.

Until the ultimate load, the bottom layer (parallel grain layer) of the slab specimen first fractured near the loading point, accompanied with a big sound, because the strain in the bottom layer reached the ultimate tensile strain of the bamboo fiber. Then, the penultimate layer (perpendicular grain layer) almost fractured at the same time due to the significantly low ultimate tensile stress compared with parallel grain layer. The cracks traced along the interface between the penultimate and third layers and propagated to the middle of the third layer. Similarly, the second layer is the perpendicular grain layer, which almost failed same as the third layer. Finally, the top layer fractured, showing the failure of the slab specimen. As shown in Figure 14, the fifteen one-way CLB slab specimens without CFRP grids had the similar failure process which was regarded as the tensile brittle failure.

For the one-way CLB slab strengthened with CFRP grids, different failure processes are obtained from groups CLB-I and CLB-M with different manufacturing processes of CFRP grids. As shown in Figures 15(a)–15(e), the failure process of group CLB-I can be summarized as follows: Cracks at the bottom layer corresponding to positions of midspan and loading points were observed when the applied load was around 140 kN. Until the load of 160 kN, the fracture of the slab specimens initiated from one of the above cracks resulted in an abrupt drop of force. The force then increased with the increase of displacement, showing the contribution of the CFRP grids for the flexural performance of the slab specimen. Until the ultimate load, the top layer of the slab specimen failed and the CFRP grids also fractured.

As shown in Figures 15(f)–15(j), there are two different failure modes for group CLB-M including (a) first bond failure at the interface of CFRP grids and bottom layer and subsequent debonding between CFRP grids and penultimate layer for CLB-M1 and CLB-M5 and (b) direct bond failure at the interface of CFRP grids and penultimate layer for CLB-M2, CLB-M3, and CLB-M4. In failure mode (a), the bamboo fibers of the bottom layer fractured first at a relatively low load, accompanied with the debonding between the bottom layer and CFRP grids. The CFRP grids and the remaining four layers still worked together until the bond failure between CFRP grids and penultimate layer occurred. After the debonding of CFRP grids and penultimate layer, the rest of the layers fractured immediately. In failure mode (b), the abrupt bond failure between the CFRP grids and

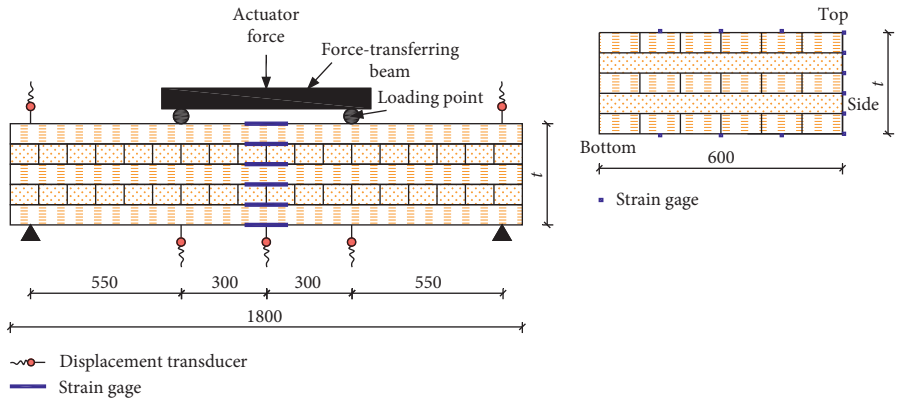

Figure 13: Layout of measurement equipment. (a) Side face. (b) Top or bottom face.

Figure 14: Failure modes of groups CLB-A, CLB-B, and CLB-C. (a) CLB-A1. (b) CLB-A2. (c) CLB-A3. (d) CLB-A4. (e) CLB-A5. (f) CLB-B1. (g) CLB-B2. (h) CLB-B3. (i) CLB-B4. (j) CLB-B5. (k) CLB-C1. (l) CLB-C2. (m) CLB-C3. (n) CLB-C4. (o) CLB-C5.

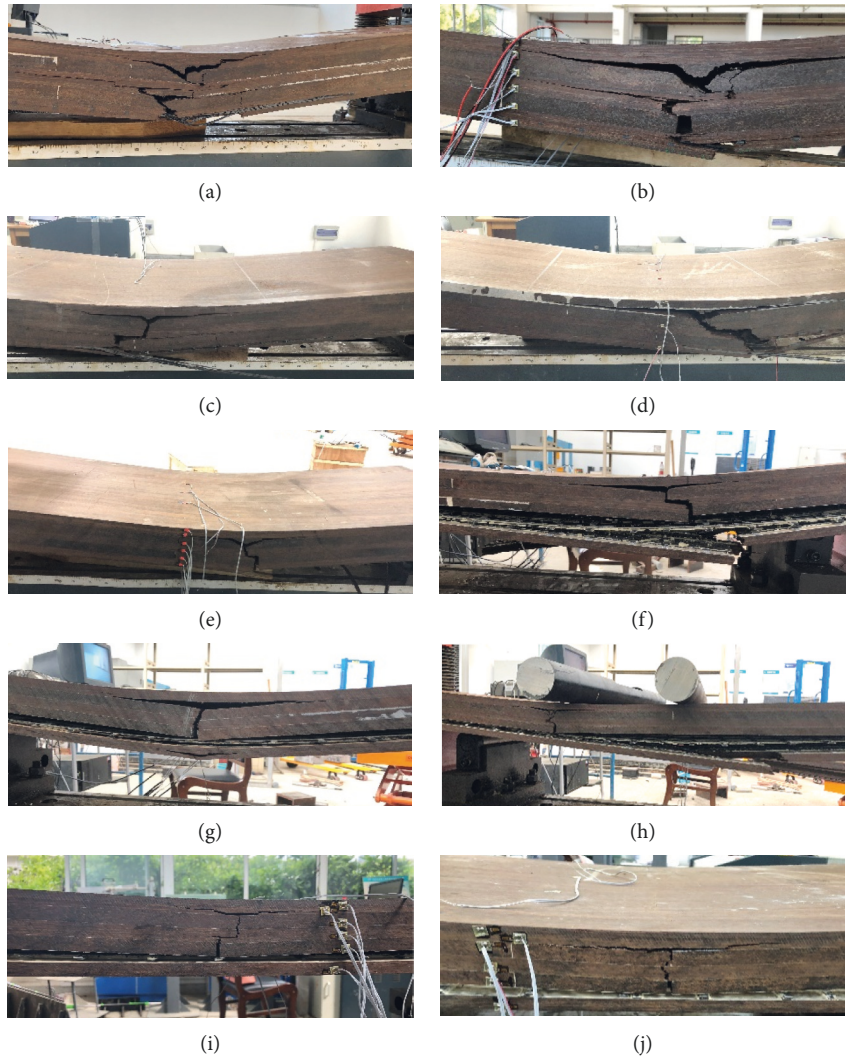

Figure 15: Failure modes of groups CLB-I and CLB-M. (a) CLB-I1. (b) CLB-I2. (c) CLB-I3. (d) CLB-I4. (e) CLB-I5. (f) CLB-M1. (g) CLB-M2. (h) CLB-M3. (i) CLB-M4. (j) CLB-M5.

penultimate layer was found around the load of 25 kN, and the rest of the four layers gradually fractured with the increase of the load.

The local drawing of failure of the slab specimens depicted in Figure 16 is to show some detailed failure positions observed in slab specimens. The separation of adjacent elements in the perpendicular grain layer was found, as shown in Figure 16(a). Accompanied with the fracture of slab layers, the debonding between the adjacent bamboo layers could be also found in Figure 16(b). For slab specimens strengthened with CFRP grids, the small cracks were found near the major crack, as shown in Figures 16(c)–16(e) clearly show the fracture of CFPR fibers and debonding of CFRP grids.

4.2. Load-Displacement Relationship. The load-midspan displacement curves of CLB slabs without CFRP grids, including groups CLB-A, CLB-B and CLB-C, are shown in Figure 17. It is obvious that the initial stage of CLB slab specimens without CFRP grids was almost linear until the elastic limit. The nonlinear behaviors were gradually found with the increase of midspan displacement, which resulted in a slow reduction of cross-sectional rigidity. The nonlinear segments in the load-midspan displacement curves of the CLB slab specimens mainly lied on the plastic compression capacity of the bamboo scrimber.

The load-midspan displacement curves obtained from slab specimens CLB-A2, CLB-B2 and CLB-C4, closest to average values of the three groups, are compared in Figure 17(d). Comparing slab specimens CLB-A2 with five 20 mm layers and CLB-C4 with five 12 mm layers, the midspan displacements of the slab specimen with thicker layers were significantly smaller than the midspan displacements of the slab specimen with thinner layers under an identical load, which demonstrated a larger cross-sectional rigidity in the slab specimen with thicker layers. Comparing slab specimens CLB-A2 with five layers and CLB-B2 with seven layers, the midspan displacements of the slab specimen with more layers were similar to those of the

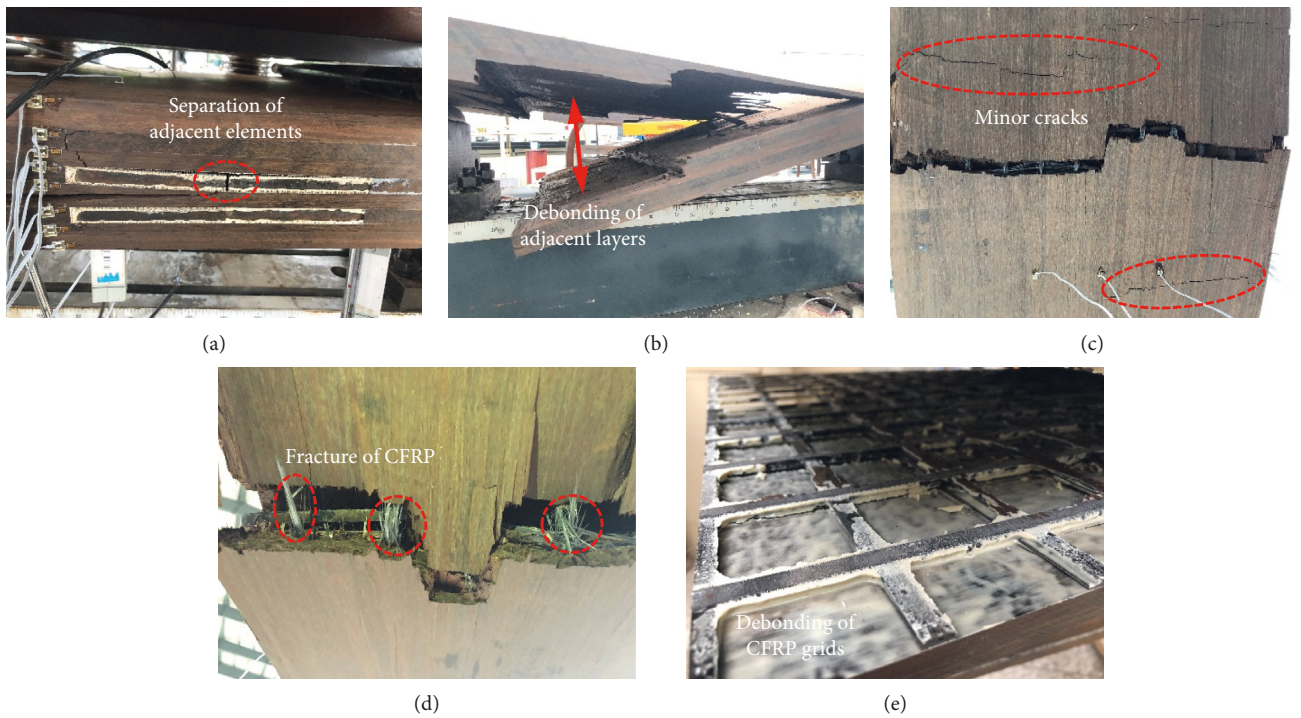

Figure 16: Local drawings of slab specimens. (a) CLB-B4. (b) CLB-C1. (c) CLB-I1. (d) CLB-I4. (e) CLB-M2.

slab specimen with fewer layer under the same load while both specimens had the same total thickness. The ductility of the slab specimens CLB-A2 and CLB-B2 with same total thickness was almost the same but was significantly smaller than that of the slab specimen CLB-C4 with smaller total thickness.

The load-midspan displacement curves of CLB slabs strengthened with CFRP grids, including groups CLB-I and CLB-M, are shown in Figure 18. Similarly, the initial stage of CLB slab specimens strengthened with CFRP grids was almost linear until the elastic limit. As shown in Figure 18(a), the significant improvement in the ductility of CLB slab strengthened with CFRP grids via manufacturing process I discussed in Section 3.1.2 was obtained compared with slab specimen CLB-A2 without CFRP grids. By introducing the CFRP grids via manufacturing process I, the midspan displacements of the slab specimen became smaller than those of the slab specimen without CFRP grids under an identical load. The cross-sectional rigidity of the slab specimen was thus found to be increased by the existence of the CFRP grids. Besides, the significant decrease of the midspan displacement near failure of the slab specimen is caused by the deviation of the displacement transducer away from the original position, as shown in Figure 18(a).

As depicted in Figure 18(b), the application of CFRP grids via manufacturing process M did not improve the flexural performance of the CLB slab specimen when comparing the slab specimen CLB-C4 and group CLB-M. Contrarily, the existence of the CFRP grids in the interface of two adjacent layers degraded the ductility of the CLB slab. The above phenomenon can be explained by the early bond failure between the CFRP grids and the bamboo scrimber layer as described in Section 4.1.

4.3. Load-Carrying Capacity. The measured ultimate loads of all tested slab specimens and the calculated average ultimate loads of each group are listed in Table 5. Because the influence of shear-span ratio on ultimate flexural bearing capacity can be neglected [43], this influence is not considered in the following comparison. The average ultimate load obtained from group CLB-C with five 12 mm layers is adopted as the reference value to evaluate the variation in the load-carrying capacity of slab specimens of different groups. Compared with group CLB-C, the groups CLB-A with thicker layers and CLB-B with more number of layers have achieved an efficient increase in ultimate load ranging from 115.5% to 165.1%. It can be found that the ultimate load of the CLB slab without CFRP grids increased with the increase of thickness of each layer and number of layers.

The average ultimate loads of group CLB-I and CLB-M are 197.4 kN and 44.3 kN, which correspond to a maximum increase of 235.7% and a decrease of 24.7%, respectively. The application of CFRP grids via manufacturing process I (pressing the CFRP grids in the bamboo layer) provided the highest improvement for the average ultimate load. For the application of CFRP grids in the interface between the bottom layer and penultimate layer, a 10% increase in the loading-carrying capacity was found in slab specimens CLB-M1 and CLB-M5, in which the bond failure first occurred at the interface of CFRP grids and bottom layer. However, in slab specimens CLB-M2, CLB-M3, and CLB-M4 with failure

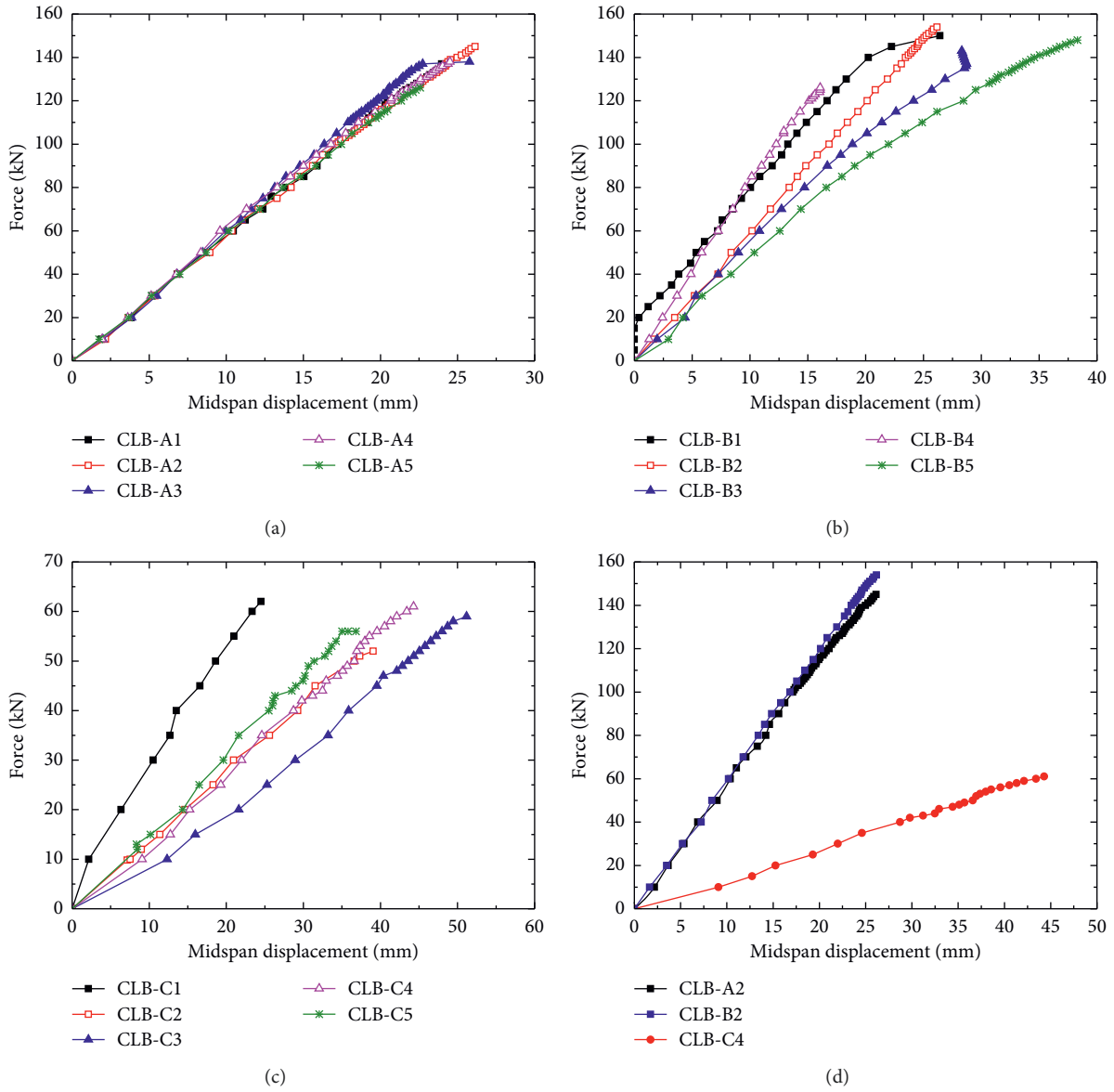

Figure 17: Load-midspan displacement curves of CLB slabs without CFRP grids. (a) Group CLB-A. (b) Group CLB-B. (c) Group CLB-C. (d) Comparison of groups CLB-A, CLB-B, and CLB-C.

mode of the direct bond failure at the interface of CFRP grids and penultimate layer, the load-carrying capacity reduced about 50%. Different interfaces, where the bond failure first occurred, affected the load-carrying capacity significantly.

4.4. Load-Strain Curves. The load-average strain relationships of slab specimens are shown in Figure 19. The tensile strain is recognized as the positive strain, which is calculated as the average value of the three strain gages attached on the bottom layer of the slab specimen. The compressive strain is defined as the negative strain, which can be obtained from the average value of the three strain gages bonded on the top layer of the slab specimen. In all slab specimens, the average strain in both tensile and compressive regions almost linearly increased with the increase of the load in the initial loading stage. Only slight nonlinearity was observed in the latter stage. Besides, the diversity of strain values obtained from different slab specimens in the same group is mainly caused by the material dispersion and local defects. As shown in Figure 19(c), the strains were abruptly changed when the bottom layer was fractured, and then the strains increased again with the load until failure.

The average ultimate tensile and compressive strains of bamboo fibers at the bottom and top surfaces are listed in Table 5. The average ultimate tensile strains of the slab specimens without CFRP grids range from 2563 $\mu\varepsilon$ and 3338 $\mu\varepsilon$, and the average compressive strains range from 2924 $\mu\varepsilon$ and 3395 $\mu\varepsilon$. The average ultimate tensile and compressive strains of the slab specimens strengthened with CFRP grids range from 2083 $\mu\varepsilon$ to 3527 $\mu\varepsilon$ and from 3557 $\mu\varepsilon$ to 5063 $\mu\varepsilon$, respectively. In general, the ultimate compressive strain was

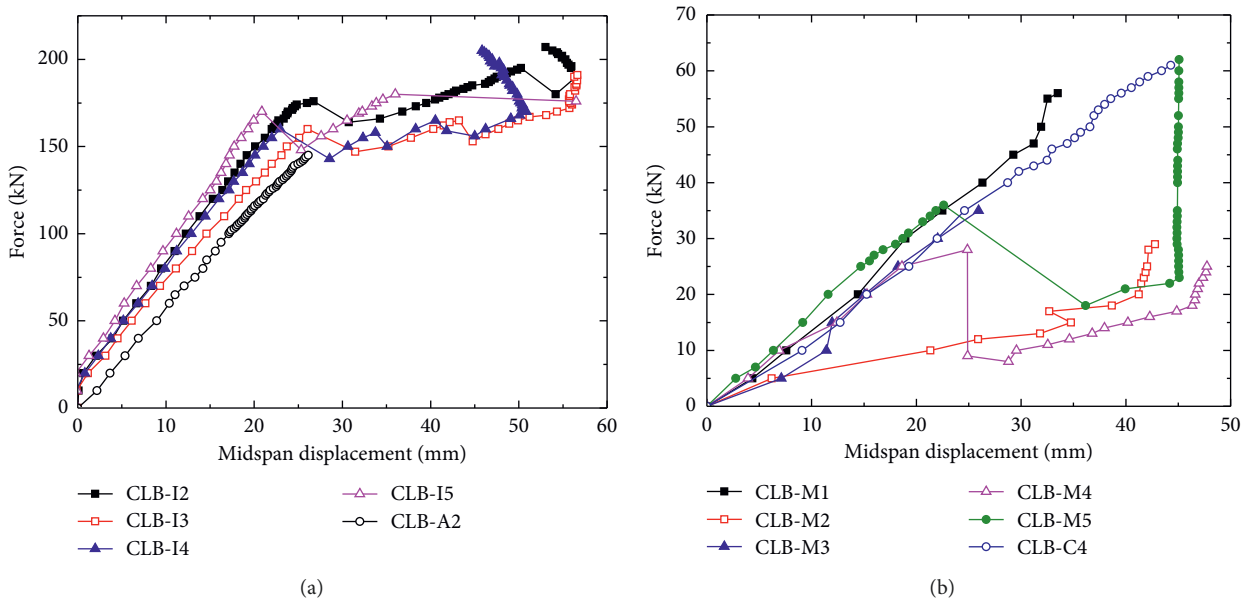

Figure 18: Load-midspan displacement curves of CLB slabs strengthened with CFRP grids.

Table 5: Test results of all specimens.

Specimen	Ultimate load (kN)	Standard deviation	Ultimate tensile strains ($\mu\varepsilon$)	Ultimate compressive strains ($\mu\varepsilon$)
Ave (CLB-A)	137.4	6.1	2889	−3395
Ave (CLB-B)	145.7	10.7	2563	−2924
Ave (CLB-C)	58.8	3.6	3338	−3156
Ave (CLB-I)	197.4	7.9	3527	−5036
Ave (CLB-M)	44.3	17.3	2083	−3557

more than the ultimate tensile strain in all slab specimens. Comparing groups CLB-A and CLB-I, the average ultimate compressive strain of the latter was 48.3% higher than the former, which demonstrated that the compressive region was utilized with more efficiency due to the employment of CFRP grids pressed in the bamboo layer. Furthermore, the average ultimate compressive strains of groups CLB-C and CLB-M were 3156 $\mu\varepsilon$ and 3557 $\mu\varepsilon$, respectively. The improvement in utilizing the compressive region via pressing in the interface was not significant.

4.5. Strain Distributions and Neutral Axis. The strain distributions along the slab thickness at the midspan cross section of representative slab specimens are shown in Figure 20. Similar to Figure 19, the positive strain is adopted as the tensile strain and the negative strain is the compressive strain. The ordinate of the curve is defined as the distance between the strain gage and bottom surface. For all representative slab specimens, the distributions of tensile strains and compressive strains are relatively symmetric. In the direction of slab thickness, the strain variation is almost linear until failure, which means that the plane cross section assumption in bending is acceptable for the one-way CLB slab and one-way CLB slab strengthened with CFRP grids in bending.

The neutral axes of slab specimens vary within the limited range near the middle height of the slab cross section. Comparing the elastic stage and the ultimate stage of the CLB slab specimens without CFRP grids, the neutral axis almost remained unchanged during the whole loading history, and only a slight upward trend of the neural axis was observed. This phenomenon demonstrated that the position of the neutral axis of the CLB slab specimen without CFRP grids was not affected by the thickness of each layer and number of layers. The slight upward movement of the neutral axis was caused by the fracture of bamboo fibers in the tension region.

As listed in Table 6, the neutral axis of the group CLB-I is lower than that of group CLB-A, and the position of the neutral axis of the group CLB-I gradually moved downward with the increase of load before failure of the bamboo layer in the bottom layer, which demonstrated that the CFRP grids sustained part of the tensile force. The existence of the CFRP grids resulted in a redistribution of stress in the cross section, and sufficient compressive behaviors in the compression region were activated. After the fracture of the bamboo fibers in the bottom layer, the neutral axis of the group CLB-I slightly moved upward.

5. Theoretical Analysis

5.1. Serviceability Limit State. According to the Chinese code GB 50005-2017 "Standard for design of timber structures" [44], the displacement limit of the slab that corresponds to the

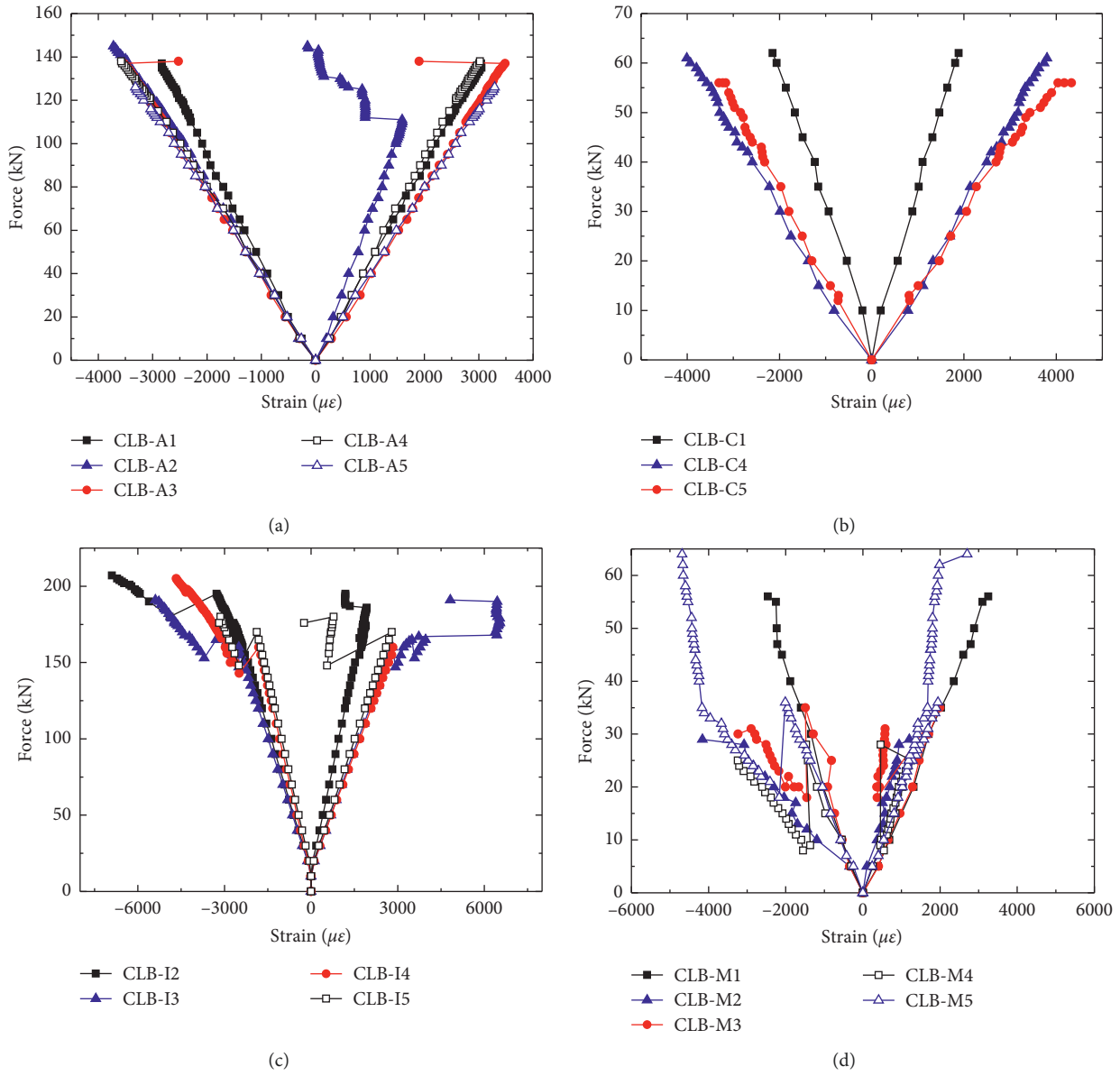

Figure 19: Load-average strain relationships of slab specimens. (a) Group CLB-A. (b) Group CLB-C. (c) Group CLB-I. (d) Group CLB-M.

serviceability limit state is prescribed as $L/250$, where L is the clear span of the slab between supports, 1700 mm in this paper. The average loads of groups CLB-A, CLB-B, and CLB-C at the midspan displacement of $L/250$ were 42.02 kN, 46.91 kN, and 9.84 kN, respectively. It is obvious that the load at the serviceability limit state increased with the increase of the layer number and layer thickness. The average loads of groups CLB-A, CLB-B, and CLB-C at the midspan displacement of $L/250$ were 61.64 kN and 8.93 kN, respectively. It is found that the CFRP grids pressed into the bottom bamboo layer can improve the load at the serviceability limit of the slab specimen significantly, but the CFRP grids bonded in the interface decreased the load at the serviceability limit.

5.2. Flexural Load-Carrying Capacity. Until now, no relevant standards and codes have been published for CLB slabs; therefore, the calculation of the flexural load-carrying capacity of the CLB slab can be referred to similar calculations of cross-laminated timber in Chinese code GB 50005-2017 "Standard for design of timber structures" [44]. The calculations of the flexural stress and effective cross-sectional rigidity are based on plane cross section assumption which is proved by the strain distribution along the slab thickness in Section 4.5. For simplicity, only layers parallel to grain are taken into consideration. The effective cross-sectional rigidity, EI_{eff}, is obtained based on the following equations:

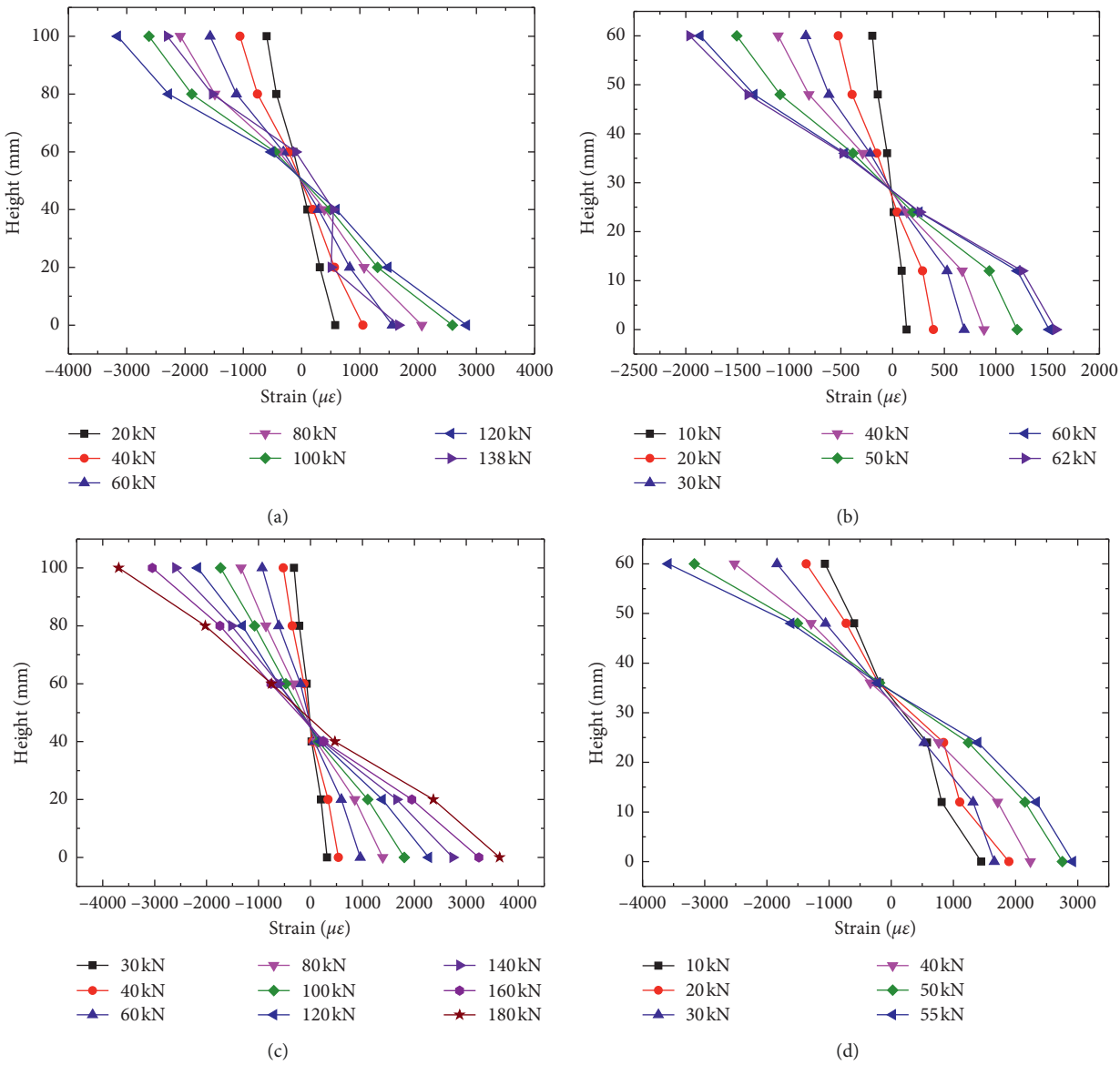

Figure 20: Strain distributions along slab thickness at midspan. (a) CLB-A3. (b) CLB-C1. (c) CLB-I2. (d) CLB-M1.

Table 6: Positions of neutral axis under different loads.

CLB-A3			CLB-I2 (before failure)			CLB-I2 (after failure)		
P	t_l	t_l/t	P	t_l	t_l/t	P	t_l	t_l/t
20	48.4	0.48	30	44.7	0.45	175	46.6	0.47
40	49.5	0.49	40	44.9	0.45	178	46.7	0.47
60	49.7	0.50	60	45.7	0.46	180	47.7	0.48
80	50.1	0.50	80	45.2	0.45	182	47.9	0.48
100	50.4	0.50	100	44.8	0.45	185	48.1	0.48
120	50.7	0.51	120	44.7	0.45			
138	56.9	0.57	140	45.5	0.45			

Note. P is the applied load; t_l is the distance between the neutral axis and the bottom surface; t is the slab thickness.

Table 7: Validation of the analytical method of calculating the flexural load-carrying capacity.

Group	P_u (kN)	M_{max} (kN·m)	EI_{eff} ($\times 10^{11}$ N·mm^2)	σ_c (MPa)	ε_{max} ($\mu\varepsilon$)	E_p (MPa)	σ_a (MPa)	Δ (%)
CLB-A	137.4	37.785	7.1082	47.71	2889	17950	51.86	8.00
CLB-B	145.7	40.0675	7.4313	48.39	2563	17950	46.01	5.18
CLB-C	58.8	16.17	1.5347	56.74	3338	17950	59.92	5.31

Note. P_u is the measured ultimate load, as listed in Table 5; M_{max} is the maximum cross section moment; σ_c is the calculated maximum flexural stress based on equation (4); ε_{max} is the average measured maximum strain, as listed in Table 5; E_p is the elastic modulus parallel to grain under tension; σ_a is the measured maximum flexural stress at failure, calculated as $E_p\varepsilon_{max}$; Δ is the error of the calculated maximum flexural stress compared with measured maximum flexural stress.

$$EI_{eff} = \sum_{i=1}^{n}\left(E_i I_i + E_i A_i e_i^2\right), \tag{1}$$

$$I_i = \frac{bt_i^3}{12}, \tag{2}$$

$$A_i = bt_i, \tag{3}$$

where E_i is the modulus of i^{th} layer parallel to grain, N/mm^2; I_i is the cross-sectional moment of inertia of i^{th} layer parallel to grain, mm^4; A_i is the cross-sectional area of i^{th} layer parallel to grain, mm^2; e_i is the distance between the centroid of i^{th} layer parallel to grain and centroid of the CLB slab, mm; b is the width of the slab, mm; t_i is the thickness of i^{th} layer parallel to grain, mm; and n is the number of layers parallel to grains. Furthermore, the flexural load-carrying capacity of the CLB slab can be calculated based on equation (4) when the span of the slab is more than 10 times the slab thickness, t:

$$\frac{ME_l t}{2EI_{eff}} \le f_{ta}, \tag{4}$$

where E_l is the elastic modulus of the outermost layer parallel to grain, N/mm^2; f_{ta} can be obtained from the ultimate tensile stress parallel to grain via coupon tests; and M is the cross section moment and is calculated as $PL_s/2$.

Based on above equations (1)–(4), the maximum tensile stress at failure can be calculated, and the comparisons between the calculated maximum tensile stress at failure and measured maximum tensile stress at failure are listed in Table 7. However, only groups CLB-A, CLB-B, and CLB-C were involved in this paper, while the groups CLB-I and CLB-M were not discussed. The main reasons are mainly explained as follows: (1) for group CLB-I, the difficulty in determining the position of CFRP grids after pressing process makes the contributions of CFRP grids for the flexural load-carrying capacity difficult to be analytically defined and (2) for group CLB-M, the unexpected bond failure occurred. Future studies will focus on the analytical model of CLB slab strengthened with CFRP grids while accurately controlling the position of CFRP grids in the CLB slab. Obviously, the accuracy of the proposed analytical method for calculating the flexural load-carrying capacity of the CLB slab is acceptable.

6. Conclusions

In this paper, five groups of one-way CLB slab specimens strengthened with or without CFRP grids, a total of twenty-five specimens, were tested under a four-point monotonic loading configuration until failure. The flexural performance of slab specimens was analyzed based on load-displacement relationship. Strain distributions in the tension and compression regions and along the side surface were monitored. Main conclusions are summarized as follows:

(1) For CLB slabs without CFRP grids, the failure initiated from the bottom layer near the loading point due to the strain in the bottom layer reaching the ultimate tensile strain and immediately propagated to adjacent perpendicular grain layer until the full failure of the CLB slab, which is regarded as tensile brittle failure. For CLB slabs strengthened with CFRP grids, different manufacturing processes resulted in different failure modes.

(2) Based on the test results, the ultimate load of CLB slabs without CFRP grids increased with the thickness of the layer and number of layers. The application of CFRP grids via pressing it into the bamboo layer significantly increased the ultimate load of slab specimen, but the CFRP grids bonded in the interface of adjacent layers negatively affected the load-carrying capacity.

(3) Based on strain analysis obtained from tension and compression regions, the linear tensile and compressive strains were observed in the initial loading stage, and the ultimate compressive strain was generally more than the ultimate tensile strain. Compared with CLB slabs without CFRP grids, a higher ultimate compressive strain was observed in CLB slabs strengthened with CFRP grids pressed in the bamboo layer, which demonstrated that the compressive region was utilized with more efficiency. Based on strain distributions along the slab thickness, the plane cross section assumption in bending is acceptable for the CLB slab with or without CFRP grids.

(4) The load at the serviceability limit state increased with the increase of the layer number, layer thickness, and CFRP grids pressed in the bamboo layer but decreased due to CFRP grids bonded in the interface. The analytical method related to flexural load-carrying capacity was proposed for CLB slabs without CFRP girds, the accuracy of which was proved.

Data Availability

All data used to support the findings of this study are available from the corresponding author upon request.

Conflicts of Interest

The authors declare that they have no conflicts of interest.

Acknowledgments

The authors would like to acknowledge the financial support from the Integrated Key Precast Components and New Wood-Bamboo Composite Structure (2017YFC0703502).

References

[1] K. S. Sikora, D. O. McPolin, and A. M. Harte, "Effects of the thickness of cross-laminated timber (CLT) panels made from Irish Sitka spruce on mechanical performance in bending and shear," *Construction and Building Materials*, vol. 116, pp. 141–150, 2016.

[2] Y. Xiao, Q. Zhou, and B. Shan, "Design and construction of modern bamboo bridges," *Journal of Bridge Engineering*, vol. 15, no. 5, pp. 533–541, 2009.

[3] E.-S. Chele, M.-C. Ricardo, P.-M. Ana, and M.-R. Teresa, "Bamboo, from traditional crafts to contemporary design and architecture," *Procedia—Social and Behavioral Sciences*, vol. 51, pp. 777–781, 2012.

[4] J. M. O. Scurlock, D. C. Dayton, and B. Hames, "Bamboo: an overlooked biomass resource?," *Biomass and Bioenergy*, vol. 19, no. 4, pp. 229–244, 2000.

[5] Y. Liao, D. Tu, J. Zhou et al., "Feasibility of manufacturing cross-laminated timber using fast-grown small diameter eucalyptus lumbers," *Construction and Building Materials*, vol. 132, pp. 508–515, 2017.

[6] Z. Wang, M. Gong, and Y.-H. Chui, "Mechanical properties of laminated strand lumber and hybrid cross-laminated timber," *Construction and Building Materials*, vol. 101, pp. 622–627, 2015.

[7] Q. Zhou, M. Gong, Y. H. Chui, and M. Mohammad, "Measurement of rolling shear modulus and strength of cross laminated timsber fabricated with black spruce," *Construction and Building Materials*, vol. 64, no. 30, pp. 379–386, 2014.

[8] Y. Wei, X. Ji, M. Duan, and G. Li, "Flexural performance of bamboo scrimber beams strengthened with fiber-reinforced polymer," *Construction and Building Materials*, vol. 142, pp. 66–82, 2017.

[9] Y. Wei, M. Zhou, and D. Chen, "Flexural behaviour of glulam bamboo beams reinforced with near-surface mounted steel bars," *Materials Research Innovations*, vol. 19, no. 1, pp. S1–103, 2015.

[10] Y. Wei, X. Ji, M. Zhou, L. Zhao, and M. Duan, "Mechanical properties of bamboo-concrete composite structures with dowel-type connections," *Transactions of the Chinese Society of Agricultural Engineering*, vol. 33, no. 3, pp. 65–72, 2017.

[11] M. Waite, "Sustainable textiles: the role of bamboo and a comparison of bamboo textile properties-Part 1," *Journal of Textile and Apparel, Technology and Management*, vol. 6, no. 2, 2009.

[12] T. Afrin, R. K. Kanwar, X. Wang, and T. Tsuzuki, "Properties of bamboo fibres produced using an environmentally benign method," *The Journal of The Textile Institute*, vol. 105, no. 12, pp. 1293–1299, 2014.

[13] C. J. Lee and J. Park, "Growth model of bamboo-shaped carbon nanotubes by thermal chemical vapor deposition," *Applied Physics Letters*, vol. 77, no. 21, pp. 3397–3399, 2000.

[14] B. Shan, L. Gao, Z. Li, Y. Xiao, and Z. Wang, "Research and applicant of solar energy-prefabricated bamboo Pole house," in *Proceedings of the 12th International Symposium on Structural Engineering*, Beijing, China, November 2012.

[15] C. Uko and N. Gowripalan, "Strength properties of raffia bamboo," *Construction and Building Materials*, vol. 3, no. 1, pp. 49–52, 1989.

[16] S. Paudel and M. Lobovikov, "Bamboo housing: market potential for low-income groups," *Journal of Bamboo and Rattan*, vol. 2, no. 4, pp. 381–396, 2003.

[17] P. J. Kaur, S. Satya, K. K. Pant, and S. N. Naik, "Eco-friendly preservation of bamboo species: traditional to modern techniques," *BioResources*, vol. 11, no. 4, pp. 10604–10624, 2016.

[18] N. Nugroho and N. Ando, "Development of structural composite products made from bamboo II: fundamental properties of laminated bamboo lumber," *Journal of Wood Science*, vol. 47, no. 3, pp. 237–242, 2001.

[19] M. Mahdavi, P. L. Clouston, and S. R. Arwade, "A low-technology approach toward fabrication of laminated bamboo lumber," *Construction and Building Materials*, vol. 29, pp. 257–262, 2012.

[20] L. Qin and W. Yu, "Research on surface color, properties of thermo-treated reconstituted bamboo lumber after artificial weathering test," *Advanced Materials Research*, vol. 79–82, pp. 1395–1398, 2009.

[21] Y. W.-J. Y. Yang-lun and Z. Y. R. Ding-hua, "Studies on factors influencing properties of reconstituted engineering timber made from small-sized bamboo," *China Forest Products Industry*, vol. 6, p. 007, 2006.

[22] B. Sharma, A. Gatóo, M. Bock, and M. Ramage, "Engineered bamboo for structural applications," *Construction and Building Materials*, vol. 81, pp. 66–73, 2015.

[23] W. Yang, J. Shenxue, L. Qingfang, Z. Qisheng, W. Libin, and L. Zhitao, "Experimental study on flexural performance of bamboo beams," *Building Structure*, vol. 1, 2010.

[24] V. De Luca and C. Marano, "Prestressed glulam timbers reinforced with steel bars," *Construction and Building Materials*, vol. 30, pp. 206–217, 2012.

[25] A. Borri and M. Corradi, "Strengthening of timber beams with high strength steel cords," *Composites Part B: Engineering*, vol. 42, no. 6, pp. 1480–1491, 2011.

[26] K. U. Schober and K. Rautenstrauch, "Post-strengthening of timber structures with CFRP's," *Materials and Structures*, vol. 40, no. 1, pp. 27–35, 2007.

[27] Y. J. Kim and K. A. Harries, "Modeling of timber beams strengthened with various CFRP composites," *Engineering Structures*, vol. 32, no. 10, pp. 3225–3234, 2010.

[28] Y.-F. Li, Y.-M. Xie, and M.-J. Tsai, "Enhancement of the flexural performance of retrofitted wood beams using CFRP composite sheets," *Construction and Building Materials*, vol. 23, no. 1, pp. 411–422, 2009.

[29] Y. Wei, S. Yan, S. Chen, M. Duan, and L. B. Wang, "Numerical simulation on bending performance of FRP reinforced bamboo beams," *Acta Materiae Compositae Sinica*, vol. 36, no. 4, pp. 1036–1044, 2019.

[30] Y. Nadir, P. Nagarajan, M. Ameen, and M. Arif Muhammed, "Flexural stiffness and strength enhancement of horizontally glued laminated wood beams with GFRP and CFRP composite sheets," *Construction and Building Materials*, vol. 112, pp. 547–555, 2016.

[31] H. Johnsson, T. Blanksvärd, and A. Carolin, "Glulam members strengthened by carbon fibre reinforcement," *Materials and Structures*, vol. 40, no. 1, pp. 47–56, 2007.

[32] H. Fang, X. Xu, W. Liu et al., "Flexural behavior of composite concrete slabs reinforced by FRP grid facesheets," *Composites Part B: Engineering*, vol. 92, pp. 46–62, 2016.

[33] R. Guo, Y. Pan, L. Cai, and S. Hino, "Bonding behavior of CFRP grid-concrete with PCM shotcrete," *Engineering Structures*, vol. 168, pp. 333–345, 2018.
[34] P. Van der Lugt, "Design interventions for stimulating bamboo commercialization-dutch design meets bamboo as a replicable model," Doctoral thesis, Delft University of Technology, Delft, Netherlands, 2008.
[35] China' National Standard, *General Requirements for Physical and Mechanical Tests of Wood (GB/T 1928:2009)*, China' National Standard, Beijing, China, 2009.
[36] China' National Standard, *Method of Testing in Tensile Strength Parallel to Grain of Wood (GB/T 1938-2009)*, China' National Standard, Beijing, China, 2009.
[37] China' National Standard, *Method of Testing in Tensile Strength Perpendicular to Grain of Wood (GB/T 14017-2009)*, China' National Standard, Beijing, China, 2009.
[38] China' National Standard, *Method of Testing in Compressive Strength Parallel to Grain of Wood (GB/T 1935-2009)*, China' National Standard, Beijing, China, 2009.
[39] China' National Standard, *Method of Testing in Compression Perpendicular to Grain of Wood (GB/T 1939-2009)*, China' National Standard, Beijing, China, 2009.
[40] Y. Li, H. Zhang, Y. Liu et al., "Synergistic effects of spray-coated hybrid carbon nanoparticles for enhanced electrical and thermal surface conductivity of CFRP laminates," *Composites Part A: Applied Science and Manufacturing*, vol. 105, pp. 9–18, 2018.
[41] X. Yang, W.-Y. Gao, J.-G. Dai, Z.-D. Lu, and K.-Q. Yu, "Flexural strengthening of RC beams with CFRP grid-reinforced ECC matrix," *Composite Structures*, vol. 189, pp. 9–26, 2018.
[42] ACI, *Guide Test Methods for Fiber-Reinforced Polymers (FRPs) for Reinforcing or Strengthening Concrete Structures (ACI 440.3R-04)*, ACI, Farmington Hills, MI, USA, 2004.
[43] J. Zhou, H. Jiang, L. Lu, Y. Qi, and Y. Zhang, "Experimental study on flexural bearing capacity of recombinant bamboo beams," *Building Structure*, vol. 23, pp. 42–45, 2016.
[44] China' National Standard, *Standard for Design of Timber Structures (GB 50005-2017)*, China' National Standard, Beijing, China, 2018.